PAPER • OPEN ACCESS

Barite concrete-based cement composites for ^{252}Cf spontaneous neutron and $^{60}Co/^{192}Ir$ shielding based on Monte Carlo computation

To cite this article: Cebastien Joel Guembou Shouop *et al* 2022 *Mater. Res. Express* **9** 045502

View the article online for updates and enhancements.

You may also like

- Peculiarities of physical and chemical processes of clinker formation in raw mixes with increased content of magnesium oxide in presence of barite waste
I N Novoselova and A G Novosyolov
- Evaluation of conversion coefficients relating air-kerma to $H^*(10)$ using primary and transmitted x-ray spectra in the diagnostic radiology energy range
J C Santos, L Mariano, A Tomal et al.
- Evaluation of mean conversion coefficients from air-kerma to $H^*(10)$ using secondary and transmitted x-ray spectra in the diagnostic radiology energy range
A H Lopez Gonzales, J C Santos, L Mariano et al.

IOP ebooks™

Bringing together innovative digital publishing with leading authors from the global scientific community.

Start exploring the collection–download the first chapter of every title for free.

This content was downloaded from IP address 41.92.186.205 on 03/05/2022 at 10:50

Materials Research Express

PAPER

Barite concrete-based cement composites for ^{252}Cf spontaneous neutron and ^{60}Co/^{192}Ir shielding based on Monte Carlo computation

Cebastien Joel Guembou Shouop[1,4,5], **Sang-In Bak**[2], **Eric Jilbert Nguelem Mekontso**[1,4], **Maurice Ndontchueng Moyo**[3,4] and **David Strivay**[5]

[1] Pure Physics Laboratory—Postgraduate Training Unit for Mathematics, Applied Computer Science and Pure Physics, University of Douala, PO Box 24157, Douala, Cameroun
[2] Korea Institute of Nuclear Safety (KINS) 62 Gwahak-ro, Yuseong-gu, Daejeon 34142, Republic of Korea
[3] Department of Physics, University of Douala, PO Box 24157, Douala, Cameroun
[4] National Radiation Protection Agency of Cameroon, PO Box 33732, Yaounde, Cameroon
[5] Atomic and Nuclear Spectroscopy, Archeometry, University of Liège, Bat. B15 Sart Tilman, 4000 Liege 1, Belgium

E-mail: sebastianguembou@gmail.com

Keywords: Monte Carlo methods, PHITS, shielding design, industrial radiography, γ-ray generation, ^{252}Cf neutron source

OPEN ACCESS

RECEIVED
21 September 2021

REVISED
9 February 2022

ACCEPTED FOR PUBLICATION
16 March 2022

PUBLISHED
6 April 2022

Original content from this work may be used under the terms of the Creative Commons Attribution 4.0 licence.

Any further distribution of this work must maintain attribution to the author(s) and the title of the work, journal citation and DOI.

Abstract

Barite concrete composite materials have been investigated for ^{252}Cf spontaneous neutron and ^{60}Co/^{192}Ir gamma sources' shielding using Monte Carlo computational method. The Particle and Heavy Ion Transport code System (PHITS) was used to compute the shielding properties of three different materials (barite concrete, barite cement, and barite aggregate) used as structural walls in fixed neutron & gamma industrial radiography for Non-Destructive Testing applications. The obtained results displayed good properties of barite concrete in shielding spontaneous neutrons emitted from the ^{252}Cf source, as the effective dose drops about 10^8 times in only 140 cm wall thickness, and it was found to be about 10 times more effective than other materials investigated. In addition, the investigated gamma shielding properties of the barite concrete showed a relatively smaller wall thickness compared to the ordinary concrete. The decision-making process based on the ALARA principle of dose limitation showed that the use of barite concrete in such facilities is more effective than the use of barite cement and barite aggregate, for both gamma and neutron radiography shielding design. To achieve an average value of 1 μSv/h, the obtained result shows that 80 cm of Barite concrete is needed, while 125 and 130 cm of barite cement and barite aggregate are needed, respectively to shield the Co-60 source. Meanwhile, 50 cm of wall made of barite concrete is sufficient to cut down the effective dose rate to 1 μSv/h (for 50 Ci and 55 cm for 150 Ci ^{192}Ir), which is an appropriate design for the public area adjacent to the industrial radiographic facility. It was therefore concluded from the obtained data that barite concrete is the most effective shielding material for radioactive sources (^{60}Co, ^{192}Ir, and ^{252}Cf) used in radiographic applications.

1. Introduction

Recently, the rapid development of neutron applications including neutron imaging, neutron radiography, neutron irradiation, …etc, has triggered different issues risen a few decades ago. In particular, neutron shielding remains a complex task in neutron applications like nuclear power reactors, fixed neutron sources for industrial radiography, and other types of neutron sources. They are slightly absorbed by heavy elements and are too sensitive to light elements such as hydrogen. The high penetration range of neutrons in high-density materials is one of the properties that make it complementary to photons (x- and gamma-rays), which are almost transparent to light elements (effective in shielding neutrons) [1, 2]. In this regard, composite cheap and temperature-resistant materials for fast neutron shielding have been developed worldwide and are still under optimization. Different materials have been investigated worldwide to determine the most appropriate material

© 2022 The Author(s). Published by IOP Publishing Ltd

Table 1. Density and the elemental composition of the investigated barite compounds and cement-based materials. The cross-section of the geometry is made of 14 layers of 10 cm each to account for the variance reduction importance in Monte Carlo calculation.

		Elemental composition								
Compound barites	Density (g cm^{-3})	H	O	Si	Al	Ca	Fe	Mg	S	Ba
Barites Cement	2.67	/	0.353	0.097	0.031	0.479	0.018	0.018	0.004	/
Barites Aggregate	2.68	0.000 98	0.304	0.0524	/	/	/	/	0.1217	0.5214
Barites Concrete	3.3	0.0055	0.322	0.042	0.002	0.041	0.084	0.003	0.087	0.364

for shielding neutron with energy below 2 MeV emitted from sources such as Am-241/Be and Am-241/Li. Many authors investigated scientific and technical neutron shielding properties of colemanite and epoxy resin, colemanite concrete, boron aggregate, colemanite, ulexite and tincal ores, and Portland cement [3–12].

Recently, Al-Buriahi *et al* reported the directly and indirectly ionizing radiation shielding properties of Fe-based alloys in the chemical composition of $Fe_{83}/B_{13-x}/C_x/Si_3/P_1$ (with x ranging from 0 to 4 mol%). He assessed the thermal and fast neutron interaction parameters in terms of scattering, absorption, and removal cross-sections using FLUKA simulations [13]. The use of new series of sodium tetraborate ($Na_2B_4O_7$) containing TeO_2, CaF_2, and CuO was developed by Sekhar *et al* and the FLUKA code was used to assess the gamma radiation transmission properties through some specimens [14]. A Saeed also investigated the neutron attenuation properties of volcanic rocks collected from the western region of Saudi Arabia and the neutron transmission factor was estimated using Monte Carlo simulations [15]. There is, therefore, a great interest in assessing radiation shielding and attenuation properties for different materials of interest worldwide. However, the optimization principle of the radiation protection system can still be implemented to increase the safety of the facility and practices that use radioactive sources as NDT testing [16–20].

Main concerns about neutron shielding related to the design of a structure to shield neutrons are structural stability, high-density material availability, and large fast-neutron removal cross-section if the source used is Cf-252. The design must be cost-benefit effective to allow its implementation in developing countries. In this regard, attention has been paid to different barite composite shielding materials and their neutron attenuation properties based on Monte Carlo calculations using Particle and Heavy Ion Transport code System [3–10]. Different types of material such as barite aggregate, barite cement, and barite concrete were investigated to find the most appropriate one for fast neutron shielding, especially spontaneous neutrons emitted from the Cf-252 source. The present study aims to provide clear recommendations for the Cf-252 spontaneous neutron source shielding in industrial radiography using barite composite materials. The investigation further evaluates the gamma shielding properties of the same material to ^{60}Co and ^{291}Ir, commonly used in gamma-ray applications such as industrial radiography, gamma imaging, and calibration.

The appropriate material composition for neutron shielding has been determined among barite composite materials investigated and compared to the previously published results related to international regulatory requirements and colemanite-peridotite concrete. Details on the computer code and the design were described. The gamma-ray source-generation from neutron absorption was discussed.

2. Barites concrete composites

Barite concrete composite materials are cementitious composites reinforced by the addition of sulfate and barium elements in a certain fraction from 0.0 to 52%. These materials are widely used for various applications of radiation shielding in nuclear engineering. They can be used for gamma-ray attenuation, neutron absorption, and low activation in shielding design, especially where fast or high-energy neutron sources are being used. While radiations as neutrons can easily damage other materials, barite composite materials were proved to be effective materials used to replace ordinary concrete in nuclear engineering [21–27]. As barite elements can be used, it is appropriate to investigate the most important parameters that influence the neutron shielding while such composite materials are used.

Cementation is also one of the newly emerging techniques for radioactive waste management as cementitious materials allow the packaging of radioactive waste with effective mechanical strength and in forms easy to handle. The description of the three composite cement-based materials used in the present study is presented in table 1, where the density varies from 2.67 to 3.30 g cm^{-3}. The elemental composition of the investigated materials is given (barites cement, barites aggregate, and barites concrete). The advantage of using barite concrete updated technology is because of their lead-free naturally occurring high-density aggregates, which can be used for concrete and pre-cast high-density concrete blocks. It is not subjected to structural concerns as water in nuclear applications as industrial radiography [16, 17, 28, 29] (water is an effective material

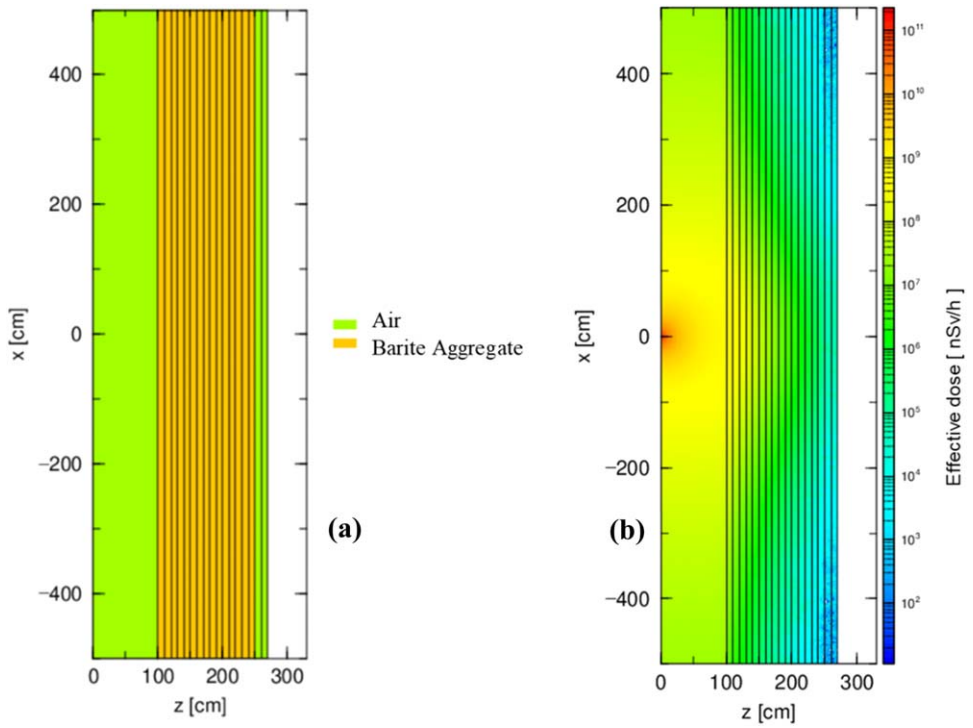

Figure 1. (a) Cross-section of the geometry used for the calculation of the radiation shielding properties of the barite aggregates and (b) the neutron flux and effective dose rate in the cross-section of the geometry.

for neutron shielding, but the shielding walls made of water are complex and not cost-effective as it poses many others issues: structure and leakage). Also, plastic materials and Paraffin could be used, but their sensitivity to fire is an important issue in heavy metal factories (with high temperatures in welding and other practices) where industrial radiography facilities are usually installed.

3. Shielding design considerations

The use of neutrons in industry, research, and medicine is still subjected to the issue of shielding which includes moderation, thermalization, and absorption of neutrons. It differs from gamma-ray shielding as the design-based maze technology was found to be effective in shielding gamma radiations [30, 31]. Though chicane design can be used for neutron, it could pose the cost-benefit effectiveness for neutron (with energy up to 20 MeV) shielding as at least 3 corners or a very lengthy maze with appropriate doors are needed to reach the desired dose level in the boundary areas (that could be possibly public areas). As the neutron's penetration power is higher than that of gamma-rays, our present concern focused on the appropriate material investigation instead of the design [16, 17, 28, 32]. The energy range emitted by a Cf-252 spontaneous neutron source reaches 20 MeV, which is higher to be cut off in the maze design without appropriate locks (neutron shielded doors). This option is economically not beneficial as the shielding equipment needed to be installed as the same as the case where chicane design is not used [17, 28, 29, 32–34].

The shielding design used in the present study was defined as a realistic case encountered in real fixed neutron radiography using ^{252}Cf sources. As the cross-section of the geometry in figure 1 displayed, the simplified geometry was made of a large test room, the walls were made of materials described in the previous section for each simulation and the tally of the dose calculation was set in the normal plan of the wall to the source. As neutron design differs from photon shielding design, the accesses design is presented in figure 2. The tally for decision-making was set outside the test room, 10 cm away from the wall. This setting was done in respect of the gamma generation from neutron absorption in the shielding material cross-section. This region was made of two cells of 10 cm thick each and filled with air (regions 17 and 18). The neutron removal cross-section of the material used is described in table 2. The geometry was set in different regions, where the first region denotes the green gap between 0 and 100 cm on the z-axis. This 1st region is followed by regions 2 to 16 as the related data will be presented in the annex section. The same geometry was used for gamma-ray emitters as Co-60 and Ir-192, though the maze design was proved to be more appropriate for gamma-ray shielding [17]. In

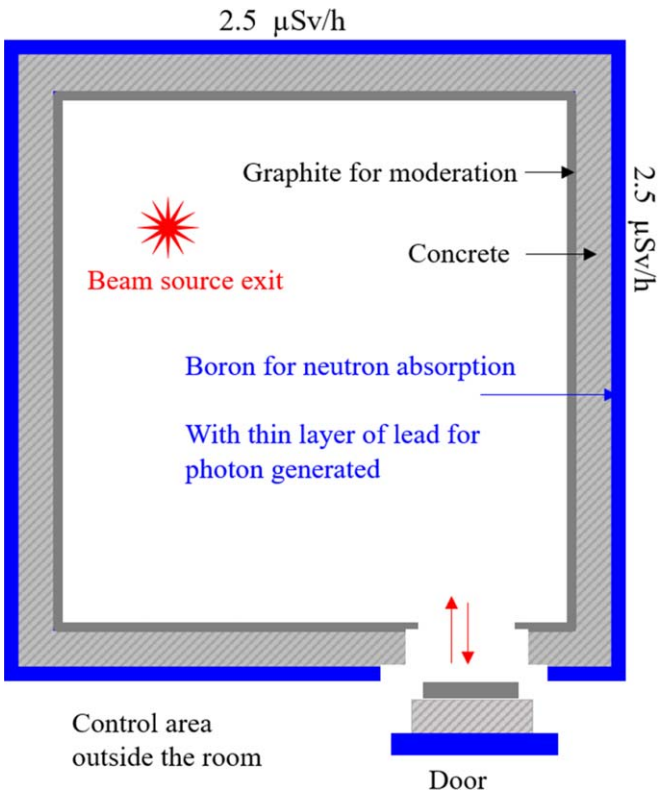

Figure 2. Design for industrial neutron radiography installation including a neutron source, walls with appropriate materials, and the main door (access) position and design. The so-called 'concrete' here refers to the three materials under investigation: barites cement, barites aggregate, and barites concrete.

Table 2. Fast-neutron removal cross-section and volumetric density of the three investigated materials.

Materials	ρ (g cm^{-3})	Σ_R (cm^{-1})	Σ_R/ρ (cm^2 g^{-1})
Barite aggregate	2.68	0.0662	0.0247
Barite cement	2.67	0.0633	0.0245
Barite concrete	3.30	0.0993	0.0301

maintaining similar geometry for both neutron and gamma shielding, it made the discussion and comparison of the obtained results more comprehensive.

4. Monte Carlo simulation

Monte Carlo techniques are computational calculations given random sampling to get reasonable statistical results that are closest to the real solution that cannot be determined statistically. The method was initially developed and presented for the Nuclear Weapon program known as the Manhattan Project, in the 1940s. Nowadays, Monte Carlo algorithms [35–38] are broadly utilized as part of tools appropriate in many fields such as chemistry, atomic, material and nuclear science, dosimetry, economics, telecommunications, and PC games... etc. Radiation attenuation through and interaction with matter is governed by attenuation coefficients or cross-sections that are probabilistic in the interaction sense. It is therefore important to use the statistical nature of radiation interaction to describe their behavior in a medium as neutrons emitted from a ^{252}Cf source are likely to interact with the medium through collision (elastic and inelastic) and absorption.

The equation of Schaeffer (1973) describes a given material effect on the fast neutron dose rate. The formula works only in certain conditions as the use of successive shielding materials including water behind a high Z material as described in the following equation [39]:

$$\dot{D}(x) = \dot{D}_0 \, e^{-\sum_R x} \tag{1}$$

Where $\dot{D}$ is the dose rate with the shielding material; $\dot{D}_0$ the dose rate without shielding material; x is the shielding material thickness (cm); and Σ_R the removal cross-section (cm^{-1})

It is usually important to multiply the previous equation by a factor B depending on the neutron energy called the buildup factor. The use of an exponential decrease equation to describe the probability of interaction is a useful tool for Monte Carlo equations' description. For instance, neutron attenuation in a medium characterized by Σ (macroscopic cross-section) is governed by the following equation [39, 40]:

$$-dI(x) = N\sigma_t\, I(x)\, dx = \sum_t I(x)\, dx \tag{2}$$

$$I(x) = I_0 \exp\left(-\sum_t . x\right) \tag{3}$$

$I(x)$ is the neutron intensity at x. Looking in term of probability, $\Sigma_t\ dx$ is the probability that a neutron will interact in the thickness dx and $\frac{I(x)}{I_0} = e^{-\Sigma_t x}$ is the probability that a neutron can move through the distance x without having a collision, the probability of the first collision at x can be defined as follow [16, 28, 32, 33, 41]:

$$p(x)\, dx = e^{-\sum_t x} \times \sum_t dx = \sum_t e^{-\sum_t x} dx \tag{4}$$

As described in the previous equation, the knowledge of Σ_t is sufficient to simulate the radiation transport in a specific material and the combination of several materials could be easily assessed as Σ is an additive operator. It is especially true when comparing the results of calculations using previous equations and experimental data. Hence, Monte Carlo methods found useful applications in radiation transport, shielding, and dosimetry. One important parameter to be considered while doing Monte Carlo simulation is the following so-called mean free path of neutron, defined as the average distance that a neutron moves between collisions [16, 42].

$$\lambda = \int_0^\infty x\, p(x)\, dx = \sum_t \int_0^\infty x\, e^{-\sum_t x} dx = \frac{1}{\Sigma_t} \tag{5}$$

Such parameters' definitions are important for Monte Carlo simulation as the interaction point and physical quantities estimated during a simulation need to be done so appropriately. Since the neutron total cross-section is complex because of the resonance area, its interaction with matter in the resonance region is not really predictable with accuracy, unless probabilistic methods are used. That is why Monte Carlo simulations are useful for such evaluations. In the present work, PHITS was used as described in the following section.

5. PHITS Monte Carlo code

The PHITS Monte Carlo code was used for simulation in the present research. It is a general-purpose Monte Carlo system developed by a collaboration between Japanese institutions and European ones. PHITS version 3.10 was used for computation, including simulation of photons and neutrons in a wide range of energy. Its use for facility shielding design and radiation protection requires proper material definition and geometry construction following a clear and well-defined method. One important parameter for accurate result definition and decision-making is the standard deviation. Different models are used to compute physical quantities in the PHITS code [43–47]. Since the shared-memory parallel computing mode was used, the relative error in the tally output file was calculated based on the following equation [17, 41, 48]:

$$\sigma = \sqrt{\frac{\sum_{i=1}^{N}(x_i w_i/\bar{w})^2 - N\bar{X}^2}{N(N-1)}} \tag{6}$$

Where N is the total batch number, x_i the tally results, w_i the source weight of each sample, $\bar{X}$ the mean value of the tally results, and $\bar{w}$ the source weight of N samples.

The PHITS input code was executed using the Radioactive decay process, a Data library from DECDC2 (Nuclear DECay Data for Dosimetry Calculation, Version 2) revised data of ICRP Publication 38 (Radionuclide Transformations - Energy and Intensity of Emissions) [18, 49, 50]. The time evolution during the simulation was not implemented as the half-life of the radionuclides used as the source is too higher than the irradiation time in the facility. For the Cf-252 neutron source, *ispfs* (self-fission source option) was specified and the source was not defined as a radioactive source, though it was the case for Co-60 and Ir-192 gamma sources. This definition fit the improved version of the code. The gamma emitters were defined in the input code as radioactive isotopes with their appropriate characteristics. The Multiplier section was set using the dose conversion coefficients for photons and neutrons from ICRP116. The importance function was used in order to get the best statistical result as shown in figure 1 (each 10 cm layer was assigned an importance). To achieve the best error estimation in this regard, the geometry of the material used was set in layers of 10 cm each and the importance was timed its value

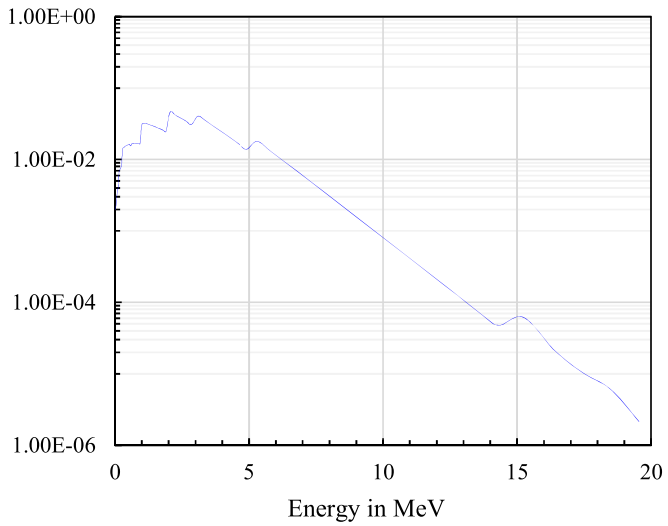

Figure 3. The Cf-252 Neutron Energy spectrum from the IAEA data library used for the present code development and computational work.

in the following layer as to compute the most important physical phenomena in the system. The Cf-252 spontaneous neutron source was disposed of in a room built for fixed neutron radiography purposes. The source consisted of 100 Ci Cf-252 in a closed facility and its neutron spectrum is displayed in figure 3. Co-60 and Ir-192 are dual energetic and multi gamma isotropic sources, with half-lives of 5.27 years and 74 days, respectively. Both are the most used source in industrial radiography because of their relatively short half-live compared to Cs-137, and high energy range compare to Se-75 and Yb-169 (32 days' half-life). Their implementation in the code was done using the radioisotope function, the point-like source geometry, and their activities.

The PHITS Monte Carlo input codes for the present study include the following sections: Title (for descriptive purpose), Parameters (major inputs for calculation modes, batches, and energy intervals and cutoff), Source (radioactive sources of gamma emitters of spontaneous neutron emitter), Material (what the geometry is made of), MatNameColor (for visual applications), Surface, Cell (volumetric geometries), T-3Dshow, Importance, 03 T-Track, Multiplier, and End [51–54]. Each T-Track section defines different physical parameters that should be extracted during the simulation in other to discuss the obtained data. The range of interest of space and energy as well as the unit of each physical parameter was set. The results presented in the following section were obtained from a validated input code [18].

6. Results and discussions

The obtained results of neutron interaction with the three types of material under investigation are shown in figures 4–7. These figures display the spatial distribution of the effective dose (μSv/h) in the tally set for this purpose. The tally for decision-making was set in the adjacent area to the irradiation room as the area is to be considered a public zone. Since most countries acknowledge the ALARA principle of dose limitation in their national regulations, this principle was used for the decision limit in the calculation using PHITS. Figure 4 shows three major sections of the effective dose calculation and these major sections are displayed in figures 5–7. The first part is characterized by the neutron interaction in the radiographic testing room filled with air, described by the tally position varying from 0 to 100 cm where the shielding wall is built. It can be seen that the effective dose variation is too low as the medium is almost transparent to spontaneous neutrons emitted from a ^{252}Cf source.

In figure 5, the three curves are overlapping in the whole geometry as we have the same medium of neutron propagation, which is air. However, between 80 and 100 cm of the tally position, there is a small variation of these three curves, representing the effective dose resulting from the use of these three materials under investigation. This small change could be explained by the scattering neutron and retro-diffusion from the shielding walls and as can be seen in figure 5, the barite concrete produces fewer secondary particles than barite aggregate and barite cement. Barite cement and barite aggregate are similar in producing secondary particles as their density and neutron shielding properties are similar.

In figure 6 the slopes of the three curves are straight (as that of a line) from 110 cm to 230 cm tally's position. This suggests the homogeneous properties of the medium the neutron is interacting with. As seen in figure 6, the highest slope is that resulting from barite concrete shielding material, followed by that of barite cement

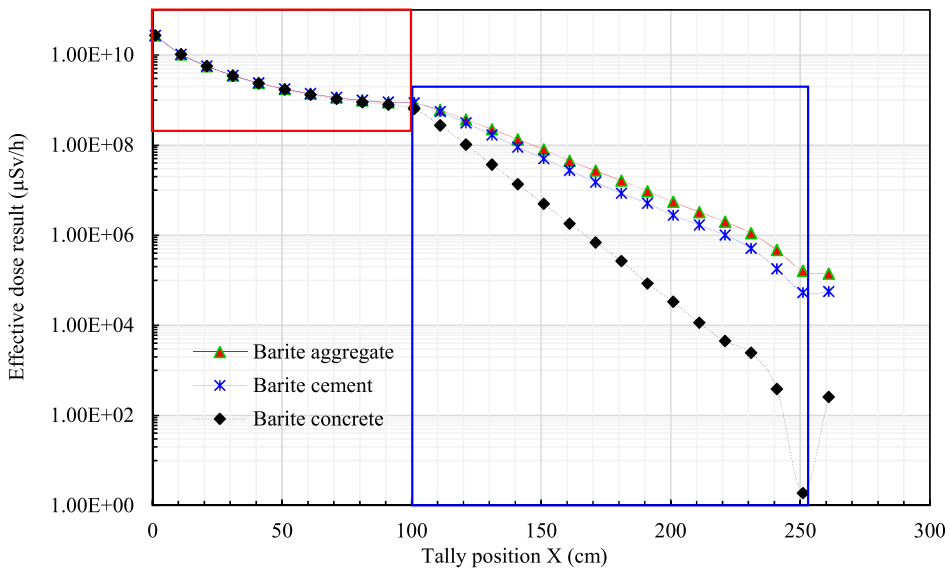

Figure 4. Results of the dose calculation for Cf-252 in the tally set for computation (cross-section of the full geometry). The first 100 cm layer represents the radiographic room air set before different walls (built in the layer between 100 and 250 cm).

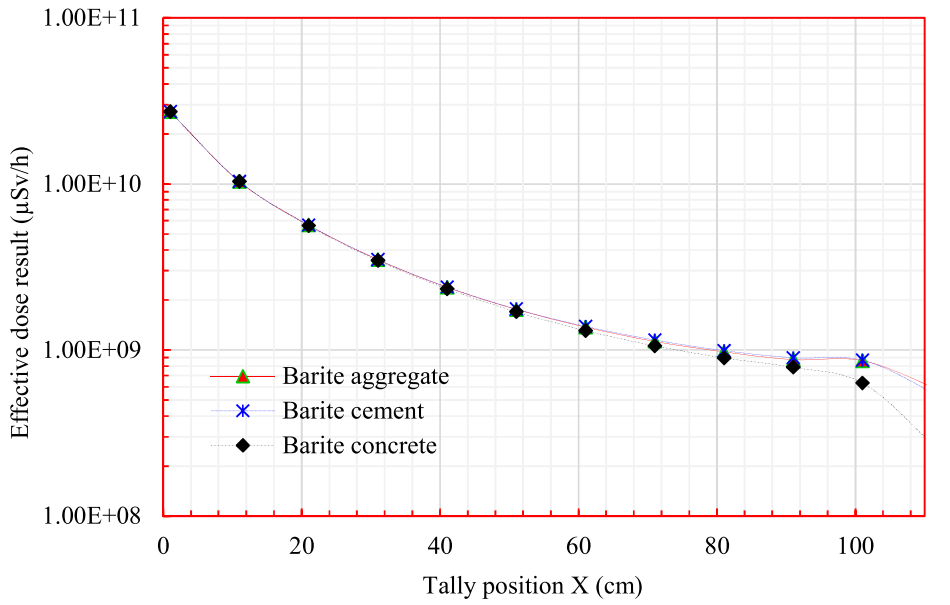

Figure 5. Results of the dose calculation for Cf-252 in the inside room tally (air) set for computation.

comparable to that of barite aggregate. This figure also displays an abrupt decrease of the effective dose rate in the latest part of the geometry from 230 to 250 cm tally's position. This is mainly due to the effectiveness of the material to slow down all fast neutrons and once the majority of spontaneous fast neutrons are slowed down to their thermal properties, they could be easily absorbed. The presence of barium in the material composition plays an important role here as neutrons could be easily absorbed within such material used for neutron absorption.

It can also be observed in the last part of the geometry (external to the radiographic test room) from 250 cm upward that there is a slight increase of the effective dose rate in the air in the adjacent region (figure 7). This is a highly interesting phenomenon we named *gamma-rays-generation from thermal neutron absorption* in the later part of the shielding walls. The gamma build-up dose generated from the thermal neutron absorption is the main cause of this phenomenon as fast neutrons are mainly slowed down before reaching the out-boundaries in the present design. The attenuation spectra of neutrons emitted from the source and the gamma-ray spectra

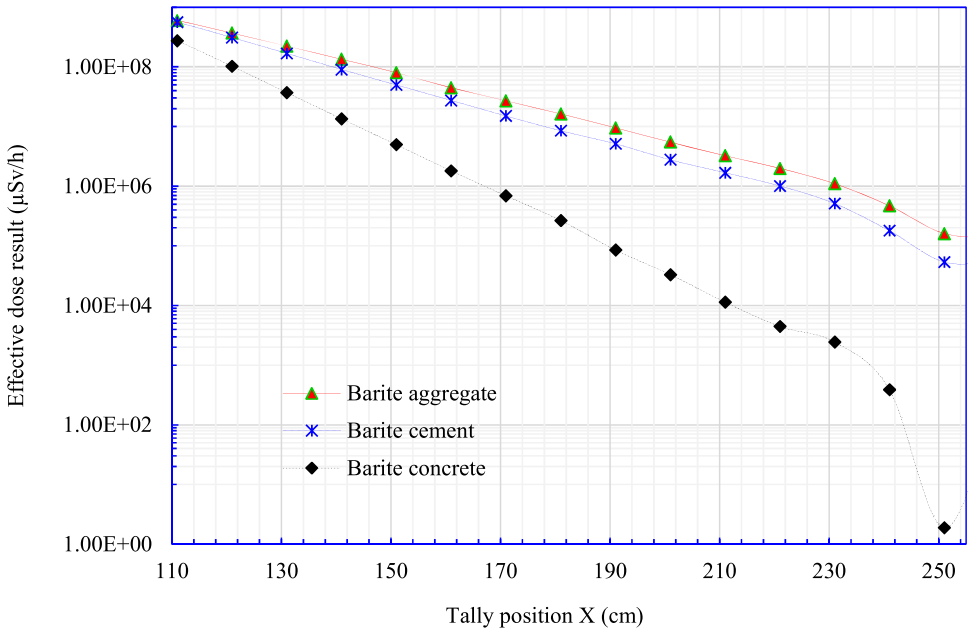

Figure 6. Results of the dose calculation for Cf-252 in the tally made off different walls (built in the layer between 110 and 250 cm). Mainly walls made of barite and concrete materials.

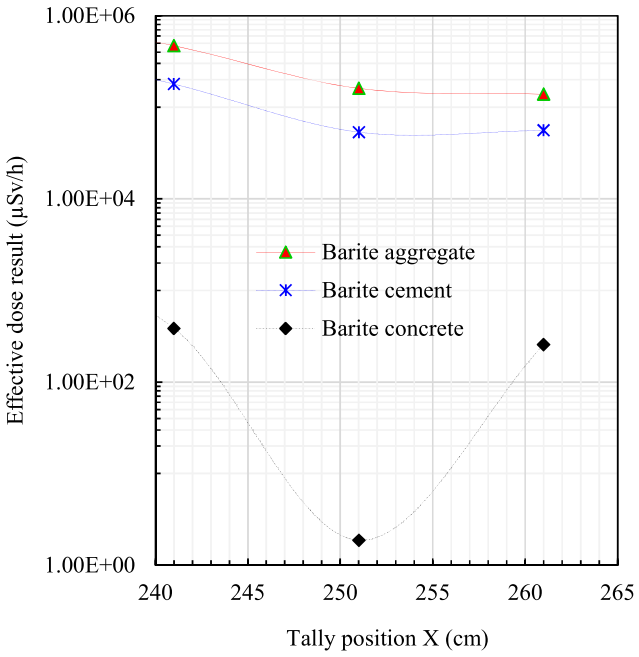

Figure 7. Results of the dose calculation for Cf-252 in the layer between 240 and 260 cm and the gamma-ray generation or buildup phenomenon from thermal neutron absorption in the latter geometry. This latter phenomenon is represented by the increase in the effective dose rate.

generated from neutron interaction can be seen in different figures in the annex section. Licenses and owners of such facilities should take into account this phenomenon in designing a fixed neutron radiographic facility as the dose rate related to neutron sources measured using a neutron detector in the adjoining area could be very low compared to the real exposure rate to radiation generated at the same area. The dose rate in the enclosing area should always take into account at least both neutron and gamma-ray components. The most effective material among the investigated ones to shield spontaneous neutrons emitted from the ^{252}Cf source is barite concrete.

The conclusion that barite concrete was found to be the most effective composite material while barite aggregate was the least effective in shielding a Cf-252 spontaneous neutron source could hardly be explained by the following reasons:

- *Material density*: While looking at material density, it can be observed that barite aggregate density is higher than that of the barite cement investigated. This leads to the observation that predicting the neutron shielding performance of material by density is inaccurate, so it is not surprising that the results are not linearly related to the material density.
- *The removal cross-section*: Barite aggregate and concrete removal cross-sections are similar and the difference observed in their effectiveness to shield Cf-252 neutron source is not controversial, but seems, unlike the expectations.
- *The amount of Ba present in a composite material*: this is one of the most important observations. The amount of Ba concentration in Barite aggregate is higher than that of barite cement and concrete. This does not support the expectation as boron and barite compounds were added to absorb thermal neutrons.

The effectiveness of barite concrete followed by barite cement could be explained by the amount of iron (Fe) in these composite materials. This is one of the main characteristics of the ^{252}Cf spontaneous neutron source with an energy spectrum that ranges from several keV to 20 MeV as the fast neutrons generated should be slowed down and thermalized prior to their absorption. The use of iron in this case is more effective in slowing down (thermalizing) neutrons emitted from ^{252}Cf and boron or borate element are effective in absorbing thermalized neutrons [16, 28, 32]. The effectiveness of different composite materials investigated is thus the result of the presence of iron in their elemental composition: Fe slows down fast neutrons at the energy appropriate for absorption by light or borate materials.

One can compare the obtained result with published ones as the main issues of designing and building a radiographic test room is safety and economic concerns. As highlighted in the introduction section, the use of water poses structural problems and leakage concerns. Plastics and paraffin are light effective neutron shielding materials but are sensitive to fire. Appropriate concrete materials such as barite concrete should be used in such industrial facilities. While the preliminary cost-benefit analysis on this barite concrete recommends its use prior to the normal concrete which poses activation concerns, other material types should be investigated for a full and complete database production. Other concrete-based materials such as the colemanite and the peridotite concrete were investigated by Koichi *et al* [55], and they obtained the neutron transmission through such material to be appropriate and that it reduced at maximum the shielding wall of about 25 cm compared to ordinary concrete [55, 56].

The following figures describe the attenuation properties of the investigated concrete to gamma radiations. As can be seen in figure 8, barite concrete is the most effective material to shield gamma-rays emitted by a Co-60 source. To achieve an average value of 1 μSv/h, the obtained result shows that 80 cm of Barite concrete is needed, while 125 and 130 cm of barite cement and barite aggregate are needed, respectively. In comparison to the previous result, these barite-based shielding materials are more effective for gamma-ray shielding.

Figure 9 shows the effective dose rate for ^{192}Ir sources of 50 and 150 Ci obtained for the same geometry. For the Ir-192, the effective dose rate was estimated for sources of 50 and 150 Ci. Once more, barite concrete was found to be the best concrete type to shield gamma-rays emitted by Ir-192 sources. As can be seen in figure 9, only a 50 cm thick wall made of barite concrete was sufficient to cut down the dose rate to 1 μSv value (50 Ci) and 55 cm was needed (for 150 Ci). It is observed that about 60 cm of barite aggregate is needed to reduce the effective dose up to 1 μSv/h. 1 μSv/h effective dose rate is obtained by setting a barite cement of 65 and 70 cm for 50 and 150 Ci, respectively. Compared to the shielding of Cf-252 source, the obtained data for gamma shows that barite concrete, barite aggregate, and barite cement are effective materials for gamma shielding and can be used for spontaneous neutron sources shielding. The obtained appropriate thicknesses to achieve the ALARA goal in the present study are lower than the previously published results for ordinary concrete by Guembou *et al* showing an improvement in the type of material used [16, 17]

7. Conclusions

The present study investigated the shielding design for spontaneous neutrons emitted from Cf-252 as well as the ^{60}Co and ^{192}Ir gamma sources used in industrial radiography. The shielding materials investigated consisted of three barite composite materials: barite cement, barite concrete, and barite aggregate. The PHITS input code was

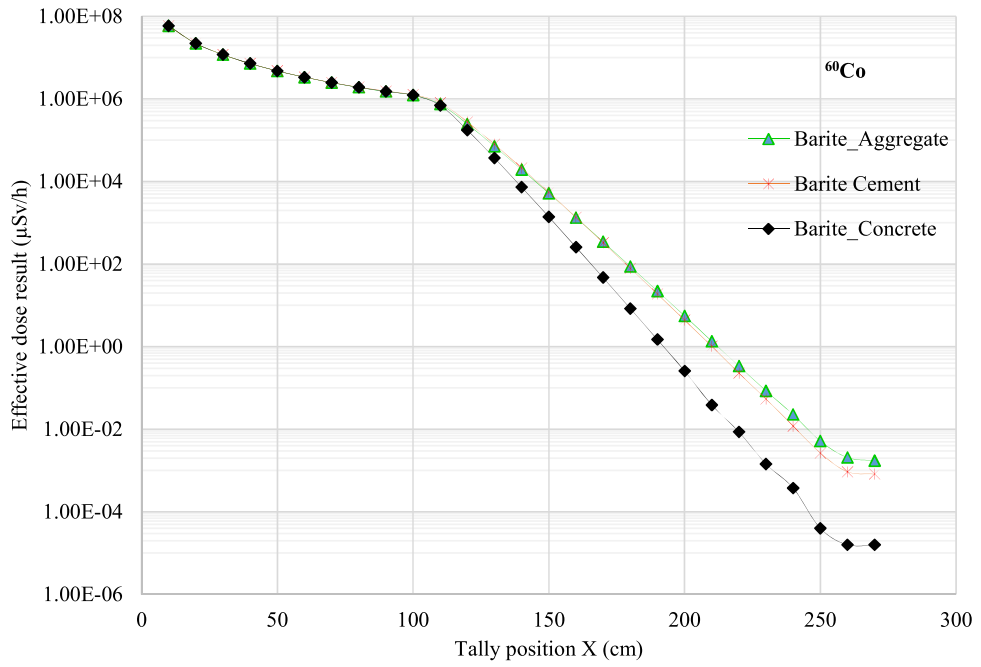

Figure 8. Effective dose rate in the geometry tally designed for ^{60}Co shielding (100 Ci). Calculation with statistical data achievement (< 5%) for the decision-making process.

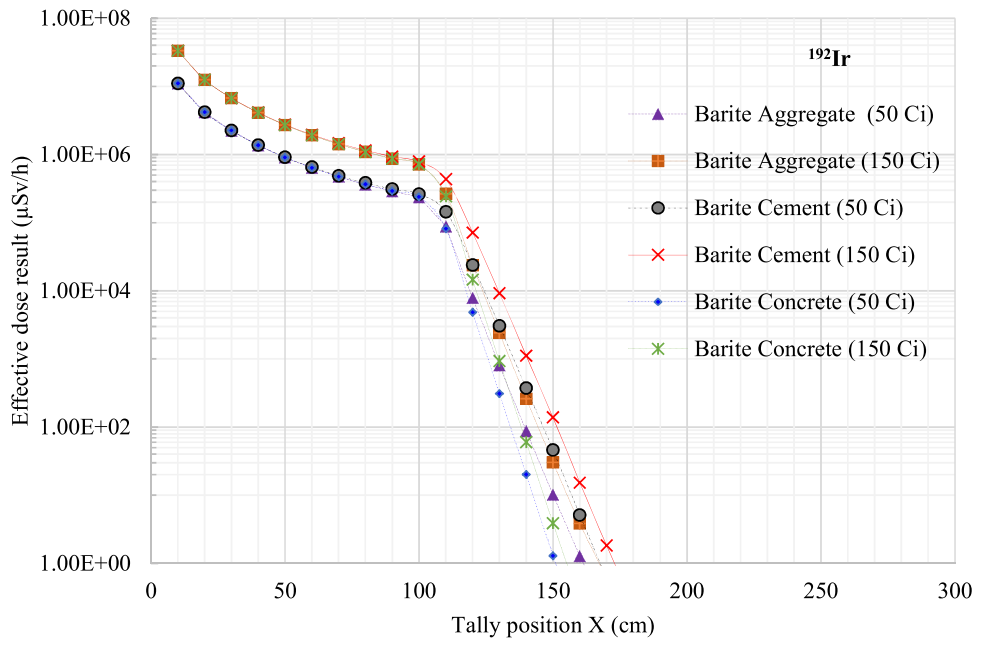

Figure 9. Effective dose rate in the geometry tally designed for ^{192}Ir shielding (150 & 50 Ci). Calculation with statistical data achievement (< 5%) for the decision-making process.

executed using the Radioactive decay process, a Data library from DECDC2 (Nuclear DECay Data for Dosimetry Calculation, Version 2) revised data of ICRP Publication 38. The appropriate material composition for neutron shielding has been determined among barite composite materials based on the generally accepted ALARA principle of IAEA. Details on the computer code and the design were described. The gamma-ray source-generation from neutron absorption was also discussed as it was found to be an interesting phenomenon. The most effective material to shield spontaneous neutrons emitted from ^{252}Cf source among the investigated ones was found to be barite concrete.

As discussed in the results section, an abrupt decrease of the effective dose rate in the latest part of the geometry from 230 to 250 cm tally's position was likely the effect of absorption of the thermalized neutron. This is mainly due to the effectiveness of the material to slow down all fast neutrons and once spontaneous fast neutrons are slowed down and thermalized, they could be easily absorbed by appropriate borate material. The combination of iron composite material and hydrogenous materials is the main reason for the effectiveness of barite concrete, followed by barite cement, and barite aggregate, respectively. The increase of the effective dose in the tally set for the decision-making process outside the radiographic test room (considered as a public area) was observed. The phenomenon was named *gamma-rays-generation from thermal neutron absorption* in the later part of the shielding walls. It was concluded that licenses and owners of such facilities should take into account this phenomenon in designing a fixed neutron radiographic facility as the dose rate related to neutron sources measured using a neutron detector in the adjoining area could be very low compared to the real exposition to radiation generated in the same area. Both ^{60}Co and ^{192}Ir gamma sources were found to be effectively shielded with a relatively small thickness of barite concrete compared to the previously published result. Therefore, it was appropriate to conclude that barite concrete is an effective material to shield both neutron spontaneous sources and gamma-ray emitters in industrial radiographic applications.

Acknowledgments

The authors are grateful to PHITS Collaboration (T Sato, S Hashimoto, K Niita, *et al*) for PHITS development, to the Korea Advanced Institute of Science and Technology—KAIST, NQE Department (Y Kim, J Park, C M Choi, *et al*) for the code license, and to the Korea Institute of Nuclear Safety—KINS (Computer Lab). They want to extend their gratitude to the National Radiation protection Agency of Cameroon—NRPA for administrative and technical support during the journey at KAIST. The authors extended their gratitude to the editorial team of the Journal of Applied Radiation and Isotopes for their positive and constructive criticism.

Data availability statement

The data that support the findings of this study are available upon reasonable request from the authors.

Declaration of competing interest

The authors declare that they have no known competing financial interests or personal relationships that could have appeared to influence the work reported in this paper.

Annex A

Spectra of photon generated from neutron interaction with the medium (in blue) and neutron spectra from the source and their attenuation throughout the geometry (in black). All the displayed figures in this annex section described gamma and neutron flux in the 14 tallies. Each spectrum displays the neutron and gamma fluxes crossing each layer of 10 cm thick material in our geometry. It can be observed that the initial neutron flux is more important than the ending one as expected while the gamma-ray flux is less important in the first tally. The main explanation is the interaction of different neutrons in the geometry and the generation of gamma as the result of neutron interaction with the medium. Gamma-rays are mainly generated in the latter part of the geometry. The graphs display the neutron and gamma-ray spectra obtained in regions 1, 2, 3, 4, 5, 6, 7, 8, 9, 10, 11, 12, 13, and 14 of the geometry presented in the 'Shielding design considerations' section.

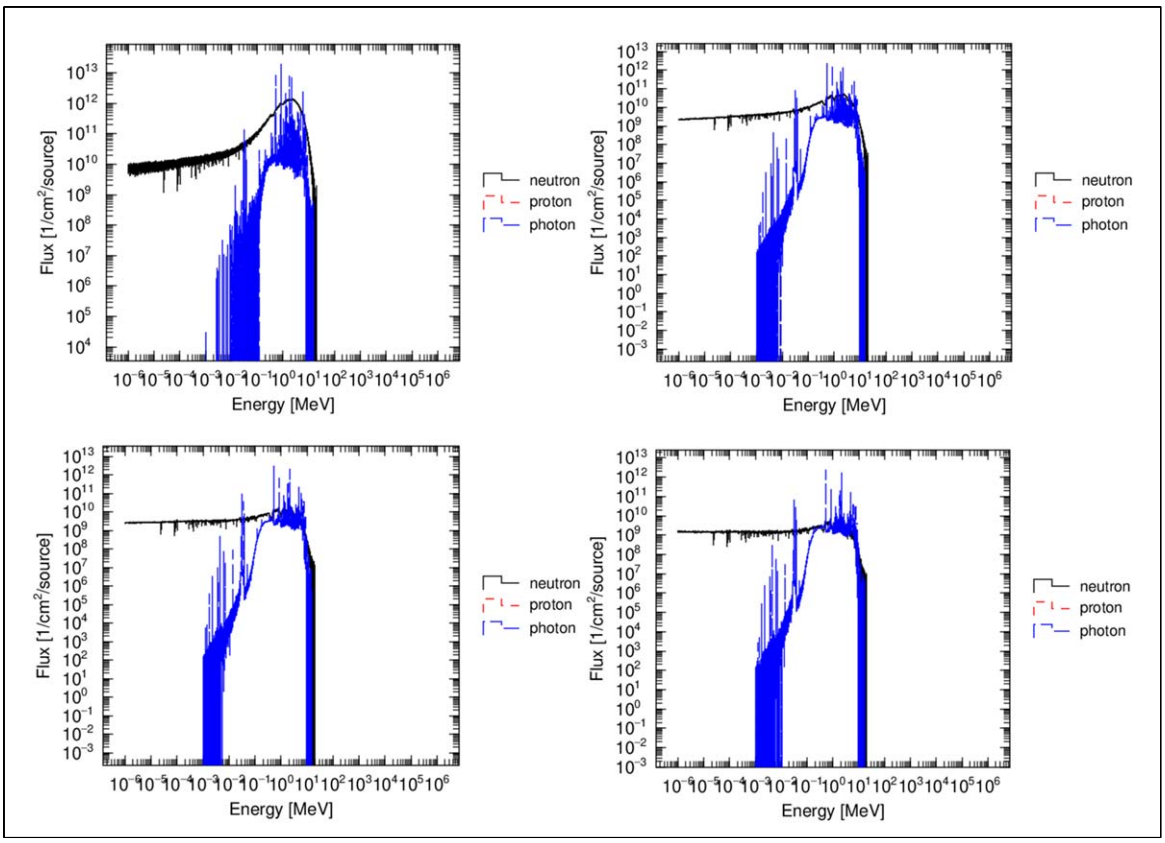
Flux [1/cm²/source]
Energy [MeV]
neutron
proton
photon

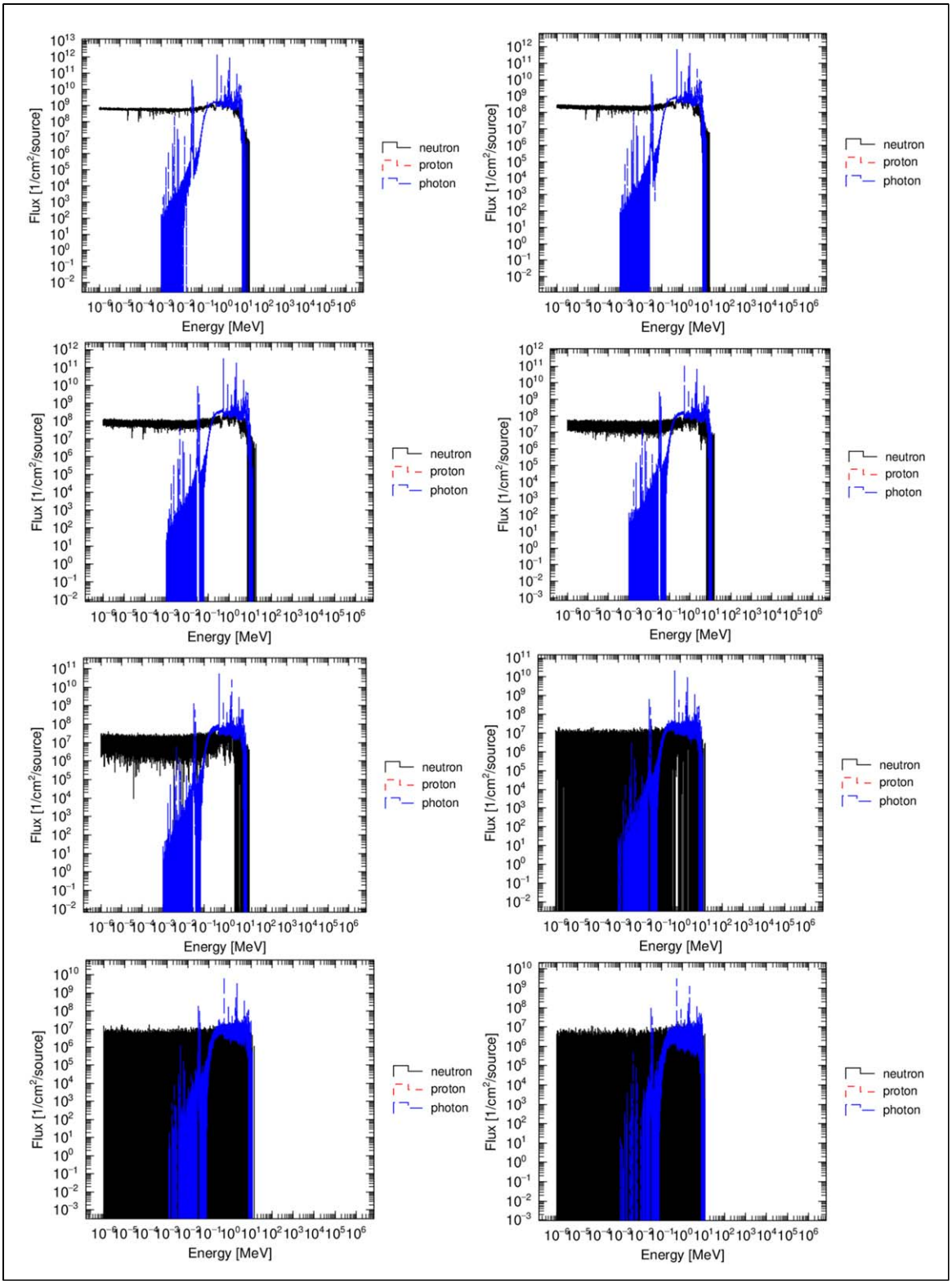
Flux [1/cm²/source]
Energy [MeV]
neutron
proton
photon

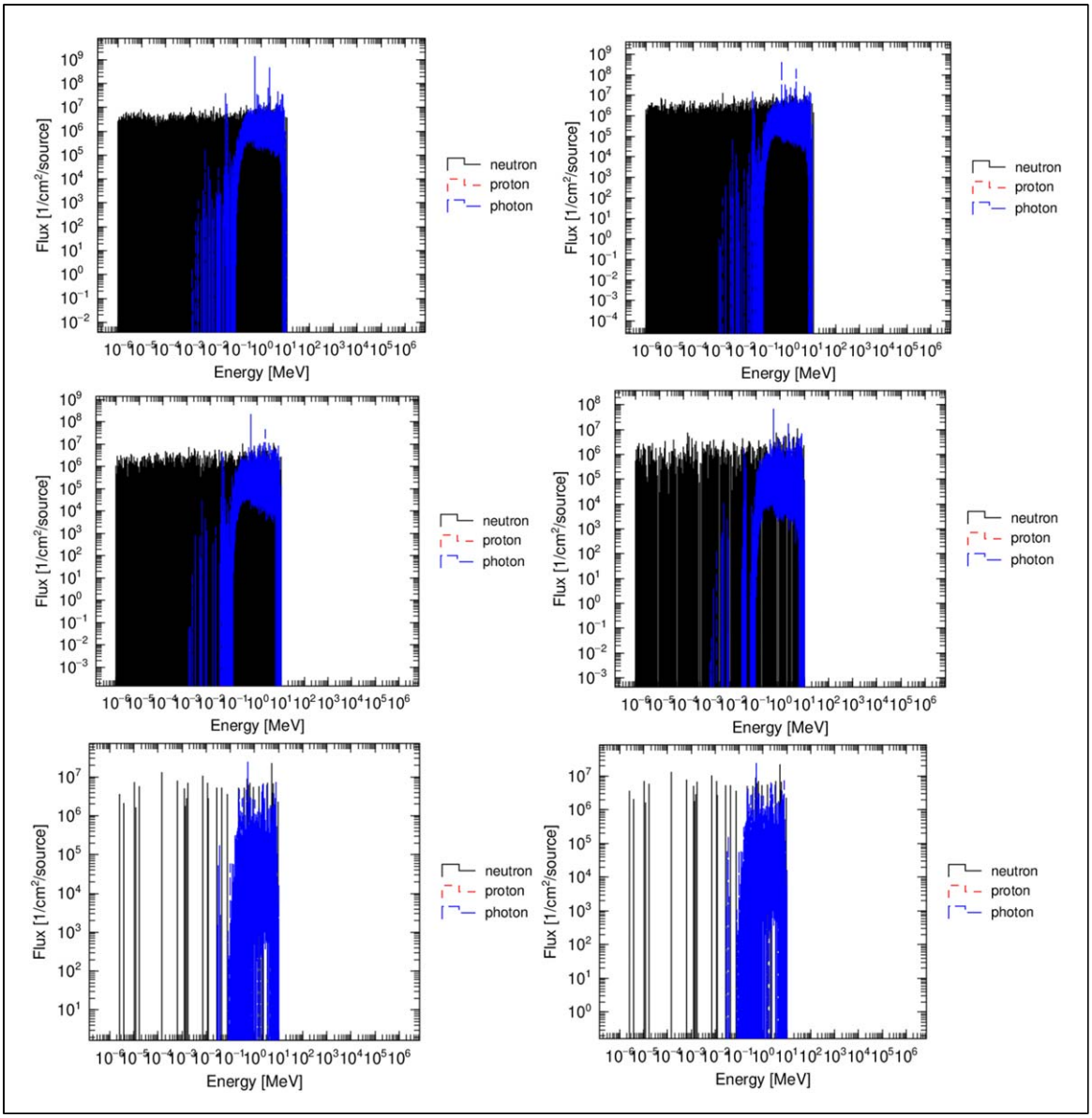

ORCID iDs

Cebastien Joel Guembou Shouop https://orcid.org/0000-0003-4740-1146

References

[1] Sowerby B D and Tickner J R 2007 Recent advances in fast neutron radiography for cargo inspection *Nucl Instruments Methods Phys Res Sect A Accel Spectrometers, Detect Assoc Equip* **580** 799–802
[2] Kardjilov N *et al* 2018 Advances in neutron imaging *Mater. Today* **21** 652–72
[3] Okuno K, Kawai M and Yamada H 2009 Development of novel neutron shielding concrete *Nucl. Technol.* **168** 545–52
[4] Kimura K I *et al* 2008 Development of low-activation design method for reduction of radioactive waste below clearance level *Int. Conf. on Nuclear Engineering, Proc.* (ICONE)
[5] Antolik A, Glinicki M A and Gawlicki M 2018 Effect of boron-containing aggregates on setting and hardening of Portland cement mortars *MATEC Web of Conferences*
[6] Yadollahi A, Nazemi E, Zolfaghari A and Ajorloo A M 2016 Optimization of thermal neutron shield concrete mixture using artificial neural network *Nucl. Eng. Des.* **305** 146–55
[7] Glinicki M A, Antolik A and Gawlicki M 2018 Evaluation of compatibility of neutron-shielding boron aggregates with Portland cement in mortar *Constr. Build. Mater.* **164** 731–8
[8] Korkut T *et al* 2012 Investigation of neutron shielding properties depending on number of boron atoms for colemanite, ulexite and tincal ores by experiments and FLUKA Monte Carlo simulations *Appl. Radiat. Isot.* **70** 341–5
[9] Korkut T *et al* 2010 Neutron dose transmission measurements for several new concrete samples including colemanite *Ann. Nucl. Energy* **37** 996–8
[10] Gencel O, Brostow W, Ozel C and Filiz M 2010 An investigation on the concrete properties containing colemanite *Int. J. Phys. Sci.*

[11] Yarar Y and Bayülken A 1994 Investigation of neutron shielding efficiency and radioactivity of concrete shields containing colemanite *J. Nucl. Mater.* **212–215** 1720–3
[12] Okuno K 2005 Neutron shielding material based on colemanite and epoxy resin *Radiat Prot Dosimetry* **115** 258–61
[13] Al-Buriahi M S *et al* 2021 Fe-based alloys and their shielding properties against directly and indirectly ionizing radiation by using FLUKA simulations *Phys. Scr.* **96** 045303
[14] Sekhar K C *et al* 2021 Synthesis, optical, and radiation attenuation properties of CaF_2-TeO_2-$Na_2B_4O_7$-CuO glass system for advanced shielding applications *Eur Phys J Plus* **136** 903
[15] Saeed A, Alomairy S, Sriwunkum C and Al-Buriahi M S 2021 Neutron and charged particle attenuation properties of volcanic rocks *Radiat. Phys. Chem.* **184** 109454
[16] Guembou Shouop C J 2020 *Shielding design and safety measures around 60Co, 192Ir, and 252Cf Sources in industrial radiography facilities based on phits Monte Carlo simulations* KAIST - Korea Advanced Institute of Science and Technology Master Thesis/1–108
[17] Guembou Shouop C J and Sang-In B 2020 Shielding design for high-intensity Co-60 and Ir-192 gamma sources used in industrial radiography based on PHITS Monte Carlo simulations *Eur. Phys. J. Plus* **135** 784
[18] Guembou Shouop C J *et al* 2022 Monte Carlo optimum management of 241Am/Be disused sealed radioactive sources *Sci. Reports* **12** 1–11
[19] Rockley J C 1977 Industrial radiography *Electron Power* **23** 321–5
[20] AGENCY IAE 1999 *Radiation Protection and Safety in Industrial Radiography* (VIENNA: IAEA) 1999 Safety Reports Series No. 13
[21] Sadeghilaridjani M *et al* 2020 Ion irradiation response and mechanical behavior of reduced activity high entropy alloy *J. Nucl. Mater.* **529** 151955
[22] Wu L *et al* 2018 Crystalline phase, microstructure, and aqueous stability of zirconolite–barium borosilicate glass-ceramics for immobilization of simulated sulfate bearing high-level liquid waste *J. Nucl. Mater.* **498** 241–8
[23] Shaaban I and Assi N 2011 Measurement of the leaching rate of radionuclide 134Cs from the solidified radioactive sources in Portland cement mixed with microsilica and barite matrixes *J. Nucl. Mater.* **415** 132–7
[24] Žagar T, Božič M and Ravnik M 2004 Long-lived activation products in TRIGA Mark II research reactor concrete shield: calculation and experiment *J. Nucl. Mater.* **335** 379–86
[25] Kareer A *et al* 2019 Short communication: 'low activation, refractory, high entropy alloys for nuclear applications *J. Nucl. Mater.* **526** 151744
[26] Wu L *et al* 2019 Microstructure, sulfate retention, and aqueous stability of barite-borosilicate glass-ceramics *J. Nucl. Mater.* **516** 152–9
[27] Nordlund K *et al* 2018 Primary radiation damage: a review of current understanding and models *J. Nucl. Mater.* **512** 450–79
[28] Guembou Shouop C J *et al* 2020 New Cf-252 neutron source shielding design based Monte Carlo simulation using material combination *AIP Adv.* **10** 075203
[29] Guembou Shouop C J *et al* 2020 Radiological protection requirements with regard to cosmic ray exposure during air travel *Eur. Phys. J. Plus* **132** 438
[30] Hu G *et al* 2020 Study on the design and experimental verification of multilayer radiation shield against mixed neutrons and γ-rays *Nucl. Eng. Technol.* **52** 178–84
[31] Issa S A M *et al* 2019 Radiation shielding and mechanical properties of Al_2O_3-Na_2O-B_2O_3-Bi_2O_3 glasses using MCNPX Monte Carlo code *Mater. Chem. Phys.* **223** 209–19
[32] Guembou Shouop C J *et al* 2020 Barite concrete for 252Cf spontaneous neutron shielding based on Monte Carlo computation *NuMat2020: The Nuclear Materials Conf.*
[33] Guembou Shouop C J and Bak S 2019 Maze influence to radiological protection around industrial radiographic sources (Co-60) under 100 Ci *Trans. of the Korean Nuclear Society Autumn Meeting Goyang (Korea, October 24-25, 2019)* pp 3–6
[34] Guembou Shouop C J *et al* 2021 Erratum to: radiological protection requirements with regard to cosmic-ray exposure during air travel *Eur. Phys. J. Plus* **136** 391
[35] Shouop G *et al* 2018 Monte Carlo method for gamma spectrometry based on GEANT4 toolkit: efficiency calibration of BE6530 detector *J. Environ. Radioact.* **189** 109–19
[36] Jenkins T M, Nelson W R and Rindi A 1988 *Monte Carlo Transport of Electrons and Photons* (US, Boston: Springer)
[37] Chiba G *et al* 2011 JENDL-4.0 benchmarking for fission reactor applications *J. Nucl. Sci. Technol.* **48** 172–87
[38] Lin Y C *et al* 2015 Monte Carlo simulations and benchmark measurements on the response of TE(TE) and Mg(Ar) ionization chambers in photon, electron and neutron beams *Nucl Instruments Methods Phys. Res. Sect. A Accel. Spectrometers, Detect Assoc. Equip.* **784** 67–73
[39] Ilboudo S D O, Sombié I, Soubeiga A K and Dræbel T 2016 Handbook of nuclear *Sante Publique (Paris)* **28** 391–7
[40] Antoni R and Bourgois L 2017 *Applied Physics of External Radiation Exposure: Dosimetry and Radiation Protection*
[41] Guembou Shouop C J *et al* 2021 241Am/Be source optimum geometry for DSRS management-based Monte Carlo simulations *AIP Adv.* **11** 115024
[42] Aygün B 2019 High alloyed new stainless steel shielding material for gamma and fast neutron radiation *Nucl. Eng. Technol.* **52** 647–53
[43] Niita K *et al* 2010 PHITS : Particle and Heavy Ion Transport code System, Version 2. 23. JAEA-Data/Code user manual Link: https://phits.jaea.go.jp/manual/manualE-phits223.pdf
[44] Niita K *et al* 2007 PHITS overview *AIP Conf. Proc.* https://inis.iaea.org/search/search.aspx?orig_q=RN:36113475
[45] Sato T *et al* 2015 Overview of particle and heavy ion transport code system PHITS *Ann. Nucl. Energy* **82** 110–5
[46] Sato T *et al* 2014 Overview of the PHITS code and its application to medical physics *Prog. Nucl. Sci. Technol.* **4** 879–82
[47] Sato T *et al* 2018 Features of particle and heavy ion transport code system (PHITS) version 3.02 *J. Nucl. Sci. Technol.* **55** 684–90
[48] Niita K *et al* 2010 PHITS : Particle and Heavy Ion Transport code System, Version 2. 23. JAEA-Data/Code https://phits.jaea.go.jp/manual/manualE-phits223.pdf
[49] Endo A, Yamaguchi Y and Eckerman K F 2005 Nuclear Decay Data for Dosimetry Calculations: Revised Data of ICRP Publication 38 https://inis.iaea.org/search/search.aspx?orig_q=RN:36113475
[50] Endo A and Yamaguchi Y 2002 Reassessment of nuclear decay database used for dose calculation *J. Nucl. Sci. Technol.* **39** 1433–6
[51] Sato T *et al* 2017 Recent improvements of particle and heavy ion transport code system: PHITS *EPJ Web of Conferences*
[52] Hashimoto S *et al* 2015 PHITS simulation of quasi-monoenergetic neutron sources from 7Li(p,n) reactions *Energy Procedia*
[53] Iwamoto Y *et al* 2017 Benchmark study of the recent version of the PHITS code *J. Nucl. Sci. Technol.* **54** 617–35
[54] Niita K *et al* 2011 Recent developments of the PHITS code *Prog. Nucl. Sci. Technol.* **1** 1–6
[55] Okuno K *et al* 2017 Development of novel neutron shielding concrete *Nuclear Technology* **168** 545–52
[56] Kawai M, Yonemura M and Kamiyama T 2020 *Development of Neutron Shielding Concrete Containing Colemanite and Peridotite* **081007** 1–12